

# Evaluation of threshold conditions for latent track formation in nanocrystalline $Y_2Ti_2O_7$

A. Ibrayeva<sup>\*,1,2</sup>, A. Mutali<sup>1,3,4</sup>, J. O'Connell<sup>1</sup>,  
A. Sohatsky<sup>4</sup>, V. Skuratov<sup>4,5,6</sup>, L. Alekseeva<sup>7</sup>,  
E. Korneeva<sup>4,8</sup>, R. Rymzhanov<sup>2,4</sup>

<sup>1</sup>Center for High Resolution Transmission Electron Microscopy, Port Elizabeth, South Africa

<sup>2</sup>Institute of Nuclear Physics, Nur-Sultan, Kazakhstan

<sup>3</sup>L.N. Gumilyov Eurasian National University, Nur-Sultan, Kazakhstan

<sup>4</sup>Joint Institute for Nuclear Research, Dubna, Russia

<sup>5</sup>National Research Nuclear University MEPhI, Moscow, Russia

<sup>6</sup>Dubna State University, Dubna, Russia

<sup>7</sup>Physico-Technical Research Institute, Nizhny Novgorod, Russia

<sup>8</sup>National University of Science and Technology NUST-MISiS, Moscow, Russia

E-mail: a.d.ibrayeva@gmail.com

DOI: 10.32523/ejpfm.2022060204

Received: 21.04.2022 - after revision

We present the first report on the structural effects induced by swift xenon ions in nanocrystalline pyrochlore  $Y_2Ti_2O_7$  (outside the metal matrix) studied using high resolution transmission electron microscopy. Latent amorphous tracks were observed in the range of electronic stopping powers 4.8–23.2 keV/nm. Obtained results enabled estimation of the threshold energy loss values for formation of continuous and not continuous (surface) tracks at  $\approx 8$  keV/nm and 3.5 keV/nm, respectively.

**Keywords:** nanocrystalline materials;  $Y_2Ti_2O_7$  pyrochlore; swift heavy ions; latent tracks; transmission electron microscopy (TEM)

## Introduction

One consequence of swift heavy ion (SHI) impact ( $E \geq 1$  MeV/nucleon) is the formation of disordered regions around the ion trajectory in the irradiated material, so-called latent tracks. Tracks are formed in many solids, particularly in dielectric crystals, due to energy deposition via electronic energy loss over a certain threshold level [1–9]. Because of the exceptional importance of such structural effects on radiation resistance, a study of the formation conditions, parameters, and morphology of tracks becomes necessary and practically valuable. In some cases, the track formation process is accompanied by phase transformations, for example, by transition from a crystalline to an amorphous state. It allows to reliably register them using various techniques, such as X-ray diffraction (XRD), Rutherford backscattering spectroscopy (RBS), and transmission electron microscopy (TEM). The latter should be highlighted as the only direct experimental method [10–12]. However, the observation of ion tracks in nanocrystalline materials can be hindered by different orientations of crystallites and/or by the background matrix influence, as typical, for example, for dielectric nanoparticles in oxide dispersion strengthened (ODS) alloys. A reduction of the incident particles' energy down to the threshold levels for track formation leads to a decrease in effective track radii and therefore a decrease in the resulting defect contrast in TEM images.

The Y-Ti-O pyrochlores are promising materials for nuclear application and hence attract special interest to study their properties under irradiation [13–24]. To date, a major part of research has been focused on nanoparticles included in ODS steels [9, 18–21]. The most detailed analysis of the radiation-induced response of  $Y_2Ti_2O_7$  pyrochlore nanoparticles in EP450 steel is presented in [9]. There the threshold ionization energy losses for track formation were found to be equal to  $S_{th} \approx 7.4\text{--}9.7$  keV/nm.

A lack of published experimental data on tracks in both bulk and isolated nanocrystalline yttrium titanate is further motivation for this work. The study aims to provide a comparative analysis of structural changes induced with high-energy heavy ion irradiation in  $Y_2Ti_2O_7$  nanooxides in isolation and embedded into a ferrite matrix.

## Materials and Methods

Nanocrystalline powder  $Y_2Ti_2O_7$  ( $\rho = 4.86$  g/cm<sup>3</sup>) was synthesized at the Research Institute of Physics and Technology of the Nizhny Novgorod State University, Nizhny Novgorod, Russia. Pyrochlore  $Y_2Ti_2O_7$  was synthesized by coprecipitation method.  $Y(NO_3)_3 \cdot 6H_2O$  (yttrium(III) nitrate hexahydrate, 99.99%) and  $TiCl_4$  (titanium(IV) chloride, 99.9%) precursors were added to distilled water to make 0.3 mol aqueous solutions. The pH of the aqueous solutions was adjusted to 8 by adding  $NH_4OH$  (ammonium hydroxide,  $\approx 25\%$ ). After that, both solutions were mixed and stirred for 20 min. The resulting mixture was evaporated at 100°C. The dry residue was annealed at 350°C, and then heated to 800°C at a rate of 5°C/min and annealed for 1 h.

The preparation of TEM specimens consisted of grinding, weighing, processing in an ultrasonic bath, and separating particles into fractions. About  $\approx 0.02$  grams of  $Y_2Ti_2O_7$  were mixed in a test tube with 10 ml of 70% alcohol for the subsequent ultrasonic processing of nanoparticle dispersions in a Bandelin ultrasonic bath (for 15 minutes at the operating frequency of 35 kHz). The accelerated sedimentation to separate particles into fractions after ultrasonic treatment by removing large particles and agglomerates was performed using an MPW-352 centrifuge, the centrifugation time was 5–10 minutes. As a result, the largest components of the solution accumulated at the tube bottom, the light ones – on the surface. A drop of this liquid was placed on a TEM grid and allowed to evaporate in a dry atmosphere.

The obtained samples were irradiated with 148 MeV Xe ions at room temperature at the IC-100 FLNR JINR cyclotron for applied research. Aluminium degraders of various thicknesses were used to vary the energy of incident ions. Uniform distribution (with an accuracy of no worse than 10%) of the ion beam over the irradiated sample surface was achieved by scanning in the horizontal and vertical directions. To prevent sample heating, the average fluences of Xe ions were less than  $10^8 \text{ cm}^{-2} \text{ s}^{-1}$ . The total ion fluence was equal to  $4 \times 10^{11} \text{ cm}^{-2}$ , which corresponds to the single track mode. Ionization energy losses  $S_e$  were calculated using the SRIM-2011 program.

The electron microscopic analysis was carried out at the Center for High-Resolution Transmission Electron Microscopy, Nelson Mandela University, Port Elizabeth, South Africa and the Flerov Laboratory of Nuclear Reactions, JINR, Dubna, Russia using JEOL ARM200F with Cs correction and Talos<sup>TM</sup> F200i S/TEM high-resolution transmission electron microscopes at 200 kV, respectively.

## Results and discussion

Visible tracks were found by TEM in samples irradiated with 148 MeV Xe ions with all aluminium degraders except  $16 \mu\text{m}$  ( $S_e \approx 1.7 \text{ keV/nm}$ ). Typical TEM images are shown in Figure 1. Tracks in  $Y_2Ti_2O_7$  are cylindrical zones of amorphous material along the incident ion trajectory.

The track sizes determined based on the contrast in TEM images and calculated values of the ionization energy loss for degraders with different thicknesses are presented in Table 1. Generally, the track formation process in yttrium titanate irradiated with SHI is very similar to the radiation response of other nanomaterials, see for instance [25, 26]. Smaller particles (sized about 20 nm) and/or thinner parts of specimens, especially close to particle borders, are more sensitive for the defect formation (Figure 2). This effect might be concerned with so-called a surface effect according to which a melting temperature can extremely decrease for a surface of particles/small particles than for bulks [27, 28]. It becomes more evident as the value of the ionization energy loss  $S_e$  is decreased.

At  $S_e \approx 4\text{--}5 \text{ keV/nm}$ , tracks are no longer seen as amorphous cylinders within the nanoparticles but instead appear as regions of defected crystal visible due to the associated strain (see Figure 3). However, the border regions and especially

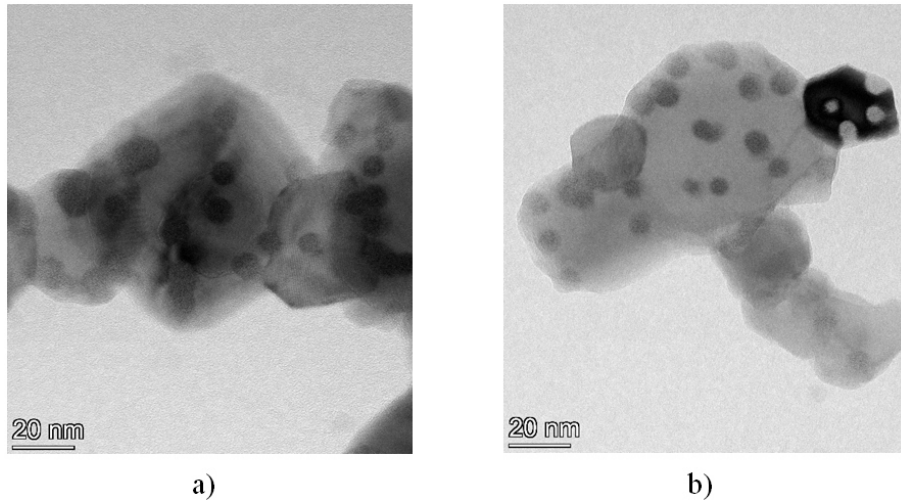


Figure 1. Bright-field TEM images of nanocrystalline  $Y_2Ti_2O_7$  irradiated with 148 MeV Xe without (a) and with 8  $\mu m$  Al degrader (b).

smaller particles do show amorphous tracks as shown in Figure 2. Very thin regions such as near the edge of a particle or within a particle of sufficiently small size places the entire interaction zone within the effective "near surface" zone [29, 30] where track formation efficiency is enhanced. Thus, this ionization energy loss should be close to the threshold level  $S_{th}$  whereas continuous tracks are formed at  $S_e \approx 8$  keV/nm and higher.

Table 1.

Parameters of irradiation with 148 MeV Xe ions and track sizes in nanocrystalline  $Y_2Ti_2O_7$ .

Ion, energy	Degrader thickness, $\mu m$	$S_e$ , keV/nm	Track diameter, $d$ , nm
Xe, 148 MeV	No	23.22	$8.9 \times 1.2$
	8	15.38	$7.6 \times 1.1$
	9.6	12.51	$6.1 \times 1.1$
	11.7	8.13	$4.2 \times 1.3$
	14	4.83	$1.5 \times 0.8^*$
	16	1.67	No tracks

\* Track size was measured only for amorphous tracks which were observed only in the smallest particles or near the edges of larger particles. In large particles tracks appeared as in Fig 3 and diameter measurement was not possible. In Figure 4 this result is marked with a green diamond.

For a more accurate assessment of the threshold values of the specific ionization energy loss for track formation in nanocrystalline  $Y_2Ti_2O_7$ , all results obtained were combined and presented as a function of  $d(S_e)$  in Figure 4. Subsequent fitting by the least-squares method made it possible to estimate  $S_{th}$  for the formation of discontinuous tracks at a level of 3.5 keV/nm. The resulting equations are shown in Figure 4. For a similar range of ionization energy losses of xenon ions  $S_e = 3.6 - 24.3$  keV/nm for nanoparticles in EP450 steel [9], the corresponding value of  $S_{th}$  was much higher  $\approx 7 - 9$  keV/nm (Figure 4). One possible

explanation of this phenomenon is that the observation of partially amorphous track regions in nanoparticles located in a metal is significantly complicated due to the influence of surrounding crystal lattice of the matrix. This does not allow to reliably determine track parameters in nanooxides in an ODS alloy close to the threshold of their formation.

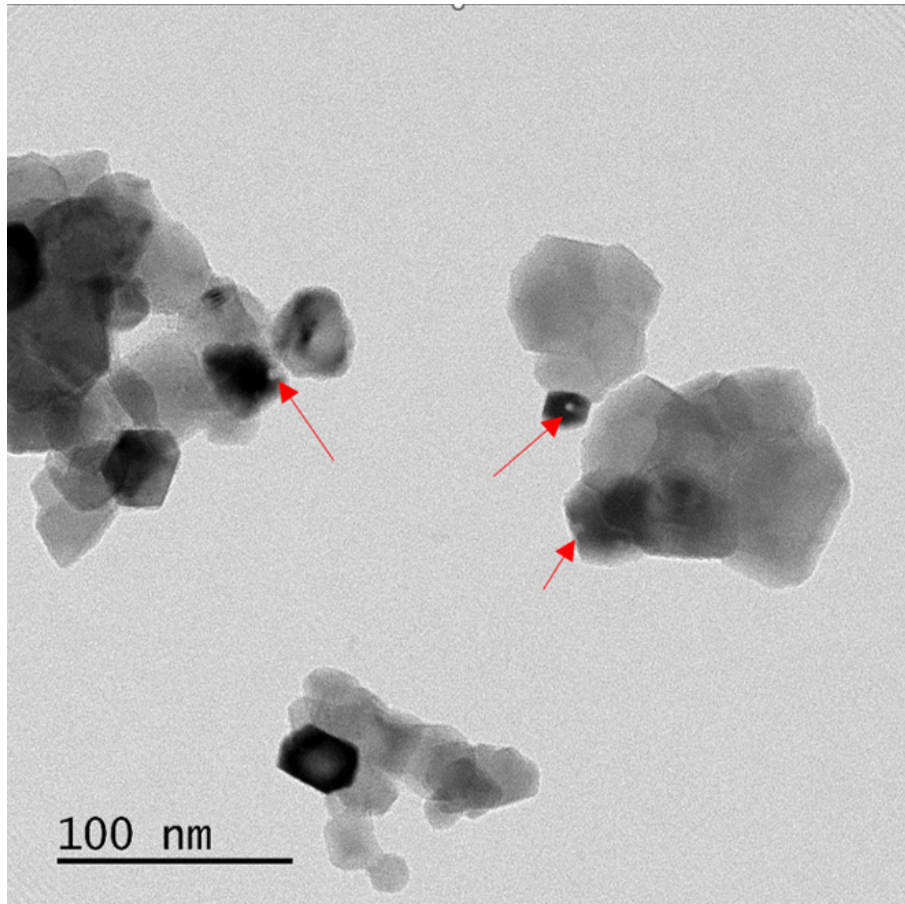


Figure 2. Bright-field TEM image of nanocrystalline  $Y_2Ti_2O_7$  irradiated with 148 MeV Xe ions with 14  $\mu m$  Al degrader ( $S_e \approx 4.83$  keV/nm).

According to the conventional thermal spike model [15, 16, 31], the formation of latent tracks in solids occurs due to a local increase in temperature to a level exceeding the melting temperature and subsequent rapid cooling. In this case it seems reasonable that isolated nanoparticles could have a lower threshold  $S_e$  for track formation compared to particles embedded in an Fe matrix since the surrounding matrix facilitated energy transport out of the particle leading to lower transient thermal spikes and thus a higher  $S_e$  is required to cause local melting. Verification of this statement based on the assumption of the dependence of track parameters on the nanoparticles size is a very complicated experimental issue due to many factors as irregular particle shapes, their different crystallographic orientation, and their boundaries imperfection.

It should be noted that at present there is no information in the literature on tracks in yttrium titanate single crystals and only one work is devoted to polycrystalline  $Y_2Ti_2O_7$  irradiated with 2.2 GeV  $^{197}Au$  ions ( $S_e = 35.7 \times 0.9$  keV/nm) [22]. The diameter of amorphous latent tracks, according to XRD analysis, was about 3–4 nm at the indicated value of the ionization energy loss. Even taking

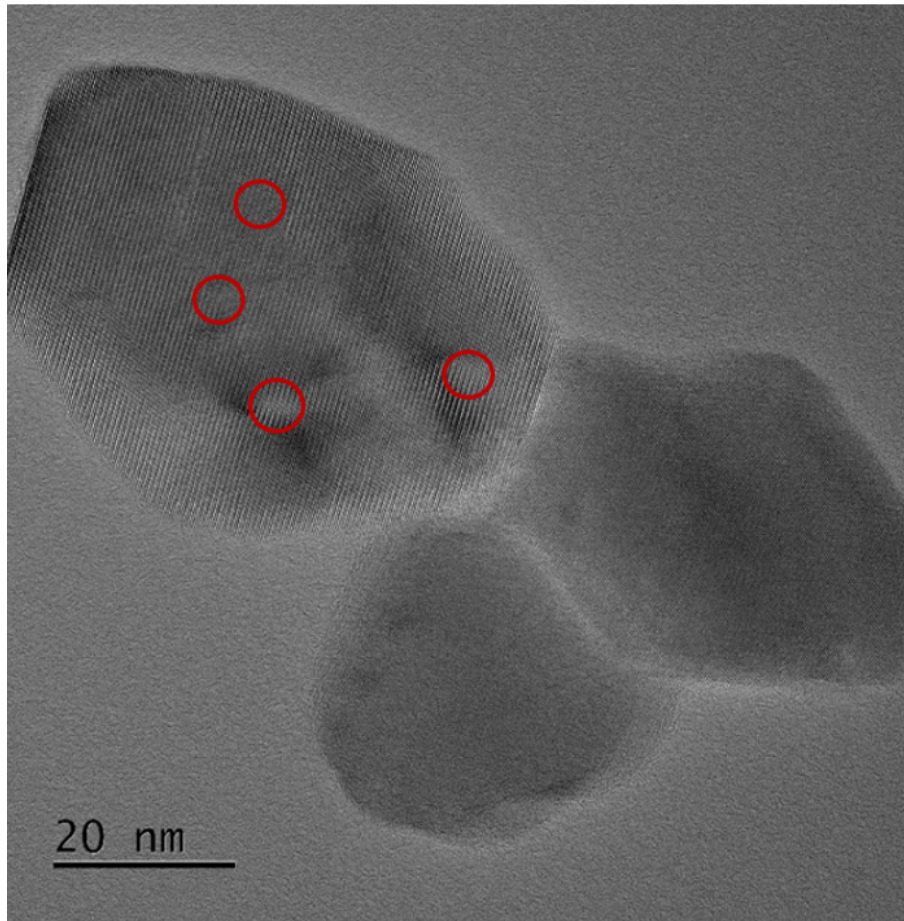


Figure 3. High resolution TEM image of nanocrystalline  $\text{Y}_2\text{Ti}_2\text{O}_7$  irradiated with 148 MeV Xe ions with 14  $\mu\text{m}$  Al degrader ( $S_e \approx 4.83$  keV/nm).

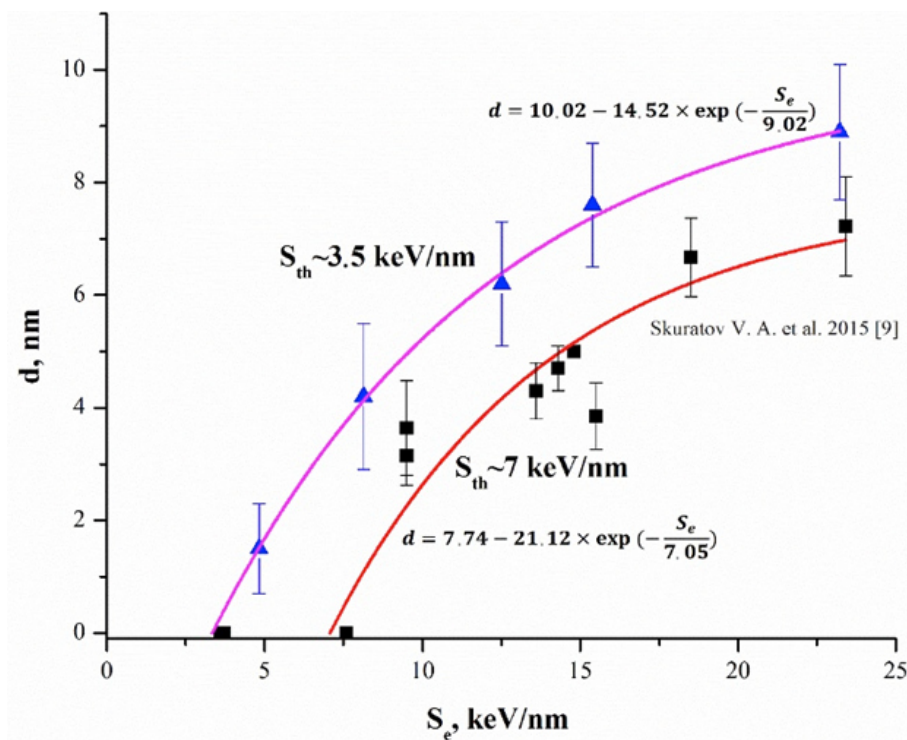


Figure 4. Dependence of the average track diameter,  $d$ , on ionization energy losses,  $S_e$ .

into account the so-called "velocity effect", which predicts a smaller track size for ions with the same energy losses but with a higher velocity [32], the average track diameter in polycrystals is much smaller than that for a nanocrystalline material. According to the available experimental data, for example, presented in [32] for  $Y_3Fe_5O_{12}$ , the track radius due to the velocity effect can differ by no more than 50%. It agrees with the suggestion that heat transfer processes in the limited volume of small particles could be considered as the main factors determining track formation thresholds. The creation of a quantitative model for such processes requires further structural electron microscopic studies and computer simulations using molecular dynamics methods.

## Conclusions

For the first time this work presents the results of studying the morphology of latent tracks induced with high-energy xenon ions in isolated  $Y_2Ti_2O_7$  nanoparticles. The threshold energy levels for formation of not continuous (surface tracks) and continuous amorphous tracks in yttrium titanate were estimated as  $\approx 3.5$  keV/nm and  $\approx 8$  keV/nm, respectively, based on analysis of high-resolution TEM images of samples irradiated in the single-track mode in the range of specific ionization energy losses  $S_e \approx 2 \div 23$  keV/nm. It is important to remember that particle size becomes an important factor determining the presence of visible tracks at  $S_e$  values near the threshold. At similar values of electron energy losses, the track diameter in isolated nanoparticles of yttrium titanate was found to be significantly larger than in similar sized nanoparticles embedded in a metal (ferrite) matrix. Parameters of the track regions are assumed to be largely determined by peculiarities of the heat transfer processes in the nanostructured material.

## Acknowledgments

This research was funded by the Ministry of Education and Science of the Republic of Kazakhstan (grant No AP09058081 "Radiation stability of dielectric nanoparticles in oxide dispersion-strengthened alloys against irradiation with heavy ions of fission fragment energy") as well as the National Research Foundation of South Africa (Grant Number 70724).

## References

- [1] S. Moll et al., Nucl. Instrum. Methods Phys. Res. B: Beam Interact. Mater. At. **268** (2010) 2933–2936. [[CrossRef](#)]
- [2] R.C. Ewing et al., J. Appl. Phys. **95** (2004) 5949–5971. [[CrossRef](#)]
- [3] S.X. Wang et al., J. Mater. Res. **14** (1999) 4470–4473. [[CrossRef](#)]
- [4] S.X. Wang et al., Nucl. Instrum. Methods Phys. Res. B: Beam Interact. Mater. At. **148** (1999) 704–709. [[CrossRef](#)]

- [5] J. Lian et al., Phys. Rev. Lett. **87** (2001) 145901. [[CrossRef](#)]
- [6] B.D. Begg et al., J. Nucl. Mater. **289** (2001) 188–193. [[CrossRef](#)]
- [7] J. Lian et al., Phys. Rev. B. **66** (2002) 054108. [[CrossRef](#)]
- [8] J. Lian et al., Acta Mater. **51** (2003) 1493–1502. [[CrossRef](#)]
- [9] V.A. Skuratov et al., J. Nucl. Mater. **456** (2015) 111–114. [[CrossRef](#)]
- [10] J.H. O’Connell et al. Acta Phys. Pol. A **136** (2019) 233–236. [[CrossRef](#)]
- [11] K. Nakajima et al., Nucl. Instrum. Methods Phys. Res. B: Beam Interact. Mater. At. **291** (2012) 12–16. [[CrossRef](#)]
- [12] A. Ibrayeva et al., Proceedings of the 14th International Conference of the Interaction of Radiation with Solids (Minsk, Belarus, 2021) 125–127.
- [13] M. Lang et al., Nucl. Instrum. Methods Phys. Res. B: Beam Interact. Mater. At. **268** (2010) 2951–2959. [[CrossRef](#)]
- [14] S. Moll et al., Nucl. Instrum. Methods Phys. Res. B: Beam Interact. Mater. At. **268** (2010) 2933–2936. [[CrossRef](#)]
- [15] G. Sattonnay et al., Nucl. Instrum. Methods Phys. Res. B: Beam Interact. Mater. At. **272** (2012) 261–265. [[CrossRef](#)]
- [16] G. Sattonnay et al., Acta mater. **61** (2013) 6492–6505. [[CrossRef](#)]
- [17] I. Jozwik-Biala et al., Acta mater. **61** (2013) 4669–4675. [[CrossRef](#)]
- [18] M.L. Lescoat et al., J. Nucl. Mater. **417** (2011) 266–269. [[CrossRef](#)]
- [19] J. Ribis et al., J. Nucl. Mater. **417** (2011) 262–265. [[CrossRef](#)]
- [20] I. Monnet et al., J. Nucl. Mater. **424** (2012) 12–16. [[CrossRef](#)]
- [21] V.A. Skuratov et al., J. Nucl. Mater. **442** (2013) 449–457. [[CrossRef](#)]
- [22] J. Shamblin et al., Acta Mater. **117** (2016) 207–215. [[CrossRef](#)]
- [23] A. Ibrayeva et al., Nucl. Mater. Energy **30** (2022) 101106. [[CrossRef](#)]
- [24] S.V. Rogozhkin et al., Nucl. Instrum. Methods Phys. Res. B: Beam Interact. Mater. At. **486** (2021) 1–10. [[CrossRef](#)]
- [25] V. Grover et al., Phys. Chem. Chem. Phys. **16** (2014) 27065–27073. [[CrossRef](#)]
- [26] W. Liu et al., Mater. **9** (2016) 105. [[CrossRef](#)]
- [27] C. Tang et al., Appl. Phys. Lett. **100** (2012) 201903. [[CrossRef](#)]
- [28] J. Lee et al., Calphad **31** (2007) 105–111. [[CrossRef](#)]
- [29] J. O’Connell et al., Phys. status solidi (b) **253** (2016) 2144–2149. [[CrossRef](#)]
- [30] R.A. Rymzhanov et al. J. Appl. Phys. **127** (2020) 015901. [[CrossRef](#)]
- [31] M. Toulemonde et al., Nucl. Instrum. Methods Phys. Res. B: Beam Interact. Mater. At. **166** (2000) 903–912. [[CrossRef](#)]
- [32] M. Toulemonde et al., Mat. Fys. Medd. **52** (2006) 263–292.